Supplementary discussion of the role of C05 HCDR1 in antigen binding. Deletion of the 5 amino-acid insertion in HCDR1 del(FGEST) and scanning mutagenesis of the tip of the loop had differing effects on binding of Fab C05 to two different H3 HAs (HK68 and Perth09). While none of these mutations had a significant effect on Fab C05 affinity for HK68 (all K_d's ~500 nM), several mutations greatly reduced C05 affinity for Perth09 (from Kd~18nM for wildtype C05 to Kd~1300nM for the del(FGEST) mutant). A large Ser159Phe substitution in Perth09 relative to HK68/H3 could enable some favorable stacking interactions with Phe27b near the tip of HCDR1 (Fig. S7). Mutating Phe27b to Ala in C05 reduced binding to Perth09 ~25-fold (460 nM), while nearby mutations in HCDR1 had no effect (Fig. 5B). None of these point mutations impacted C05 binding to HK68/H3, suggesting that all mutants are functional. In addition, non-conservative mutations of Tyr31, which supports the elongated HCDR1 loop, greatly impairs C05 binding to Perth09, but has no effect on binding to HK68/H3 (Fig. 5B). Mutations on Perth09 HA are consistent with Tyr31 acting to support the HCDR1 loop conformation, rather than making important direct interactions with HA (Fig. S8). On the whole, these data suggest that while HCDR1 may increase the affinity of C05 against some targets, HCDR3 alone is sufficient for C05 activity.

Supplementary discussion on the functional assessment of C05 HCDR3 peptides. C05 utilizes its long HCDR3 to bind the receptor binding site of multiple influenza subtypes and prevent their cellular attachment. This extensive interaction of a single CDR with the binding site suggested that peptides based on the HCDR3 sequence may also prevent HA binding to its receptor. To explore this possibility, we synthesized peptides based on the C05 HCDR3 that allow investigation of the free peptide, a di-cysteine cyclized variant, avid display through a single biotin coupled with streptavidin, and a streptavidin-constrained di-biotin variant. None of these peptides with or without streptavidin were able to inhibit hemagglutination to a detectable level (data not shown). These results suggest that the antibody context is important for the proper display of the C05 HCDR3, as outlined in the main text. A

description of the method and a list of the peptide sequences follow.

Functional assessment of peptides that comprise the C05 HCDR3 were synthesized (ELIM Biopharma) as free peptides or singly or double biotinylated to allow analysis as multivalent complexes or constrained structures using streptavidin. Peptides were dissolved in DMSO and diluted into PBS with or without recombinant streptavidin (Thermo) at a 4:1 peptide to streptavidin ratio followed by serial half log dilutions to cover a range of 150- 0.14 ug/ml in duplicate. The peptide mixtures were then incubated with 4 hemagglutinating units of H1N1 New Caledonia/20/1999 inactivated virus (Meridian Bioscience) for 1 hour, followed by addition to 0.5% chicken red blood cells in Alsever's solution (Lampire) in a V-bottom 96-well assay plate. The mixture was incubated an additional 30 minutes at room temperature followed by centrifugation at 300X g for 5 minutes to pellet non-hemagglutinated cells. For controls, PBS with DMSO with and without streptavidin, and C05 IgG were used. Only wells receiving control agents formed buttons of precipitated chicken RBCs after centrifugation, all other wells contained hemagglutinated RBCs. The experiment was performed twice with similar results.

C05 HCDR3 peptide sequences
AKHMSMQQVVSAGWERADLVGDAFDGG
cAKHMSMQQVVSAGWERADLVGDAFDcGG-NH-Biotin Cyclized
cAKHMSMQQVVSAGWERADLVGDAFDGG-NH-Biotin
Biotin-AKHMSMQQVVSAGWERADLVGDAFDGG-NH-Biotin

a

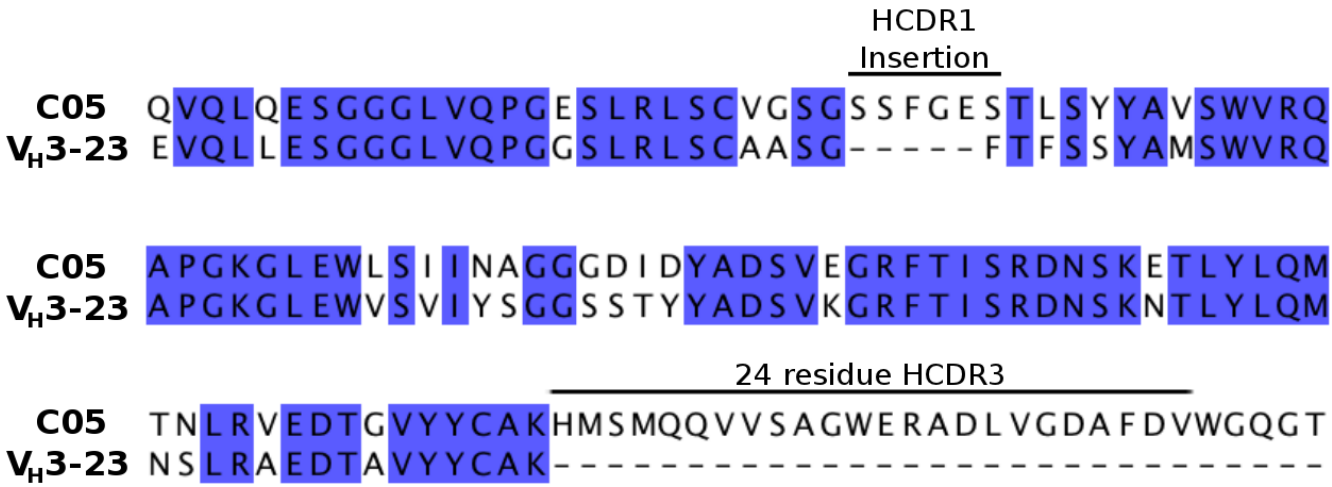

b

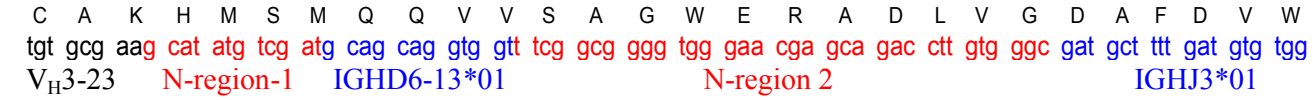

Total gene derived nucleotides= 30
Total non-gene derived nucleotides= 46

Supplementary Figure 1: C05 has a long HCDR3 and a somatic insertion in HCDR1. a, Alignment of C05 and the germline V_H3-23 sequence, with the 5 amino-acid insertion in HCDR1 and the 24-residue long HCDR3 indicated. Residues shared between the germline and C05 are highlighted in blue, with differing positions in white. **b**, Sequence of the V-D-J junction of C05, with putative gene segments and N-regions indicated. In addition to V_H3-23, the C05 heavy chain uses IGHD6-13*01 and IGHJ3*01 (although IGHJ4*01, IGHJ4*02, or IGHJ4*03 may also be possible).

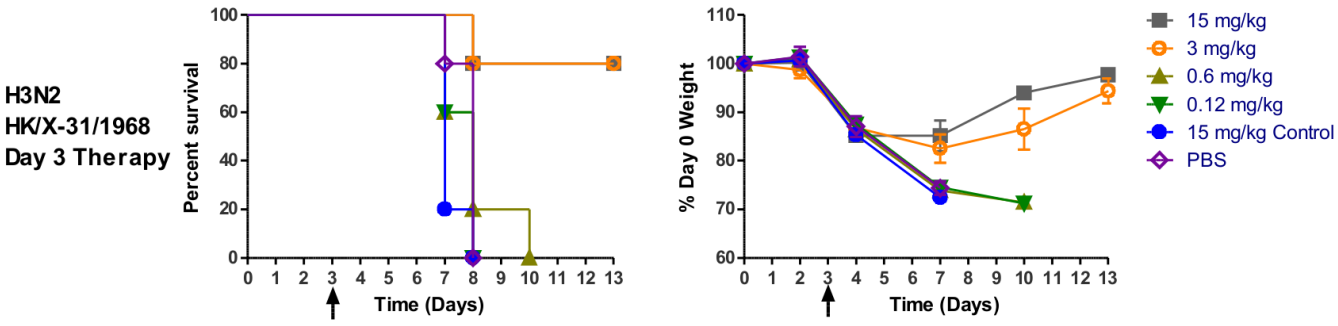

Supplementary Figure 2: Minimum therapeutic dose of C05 IgG required for protection. Mice were challenged with 33 MLD_{50} of A/Aichi/2/X-31/1968 (H3N2) virus and increasing amounts of C05 IgG was administered 3 days post-infection (arrow). A single dose of 3 mg C05 IgG 3 days post-infection was sufficient to protect 80% of the mice. Left, survival. Right, weight loss.

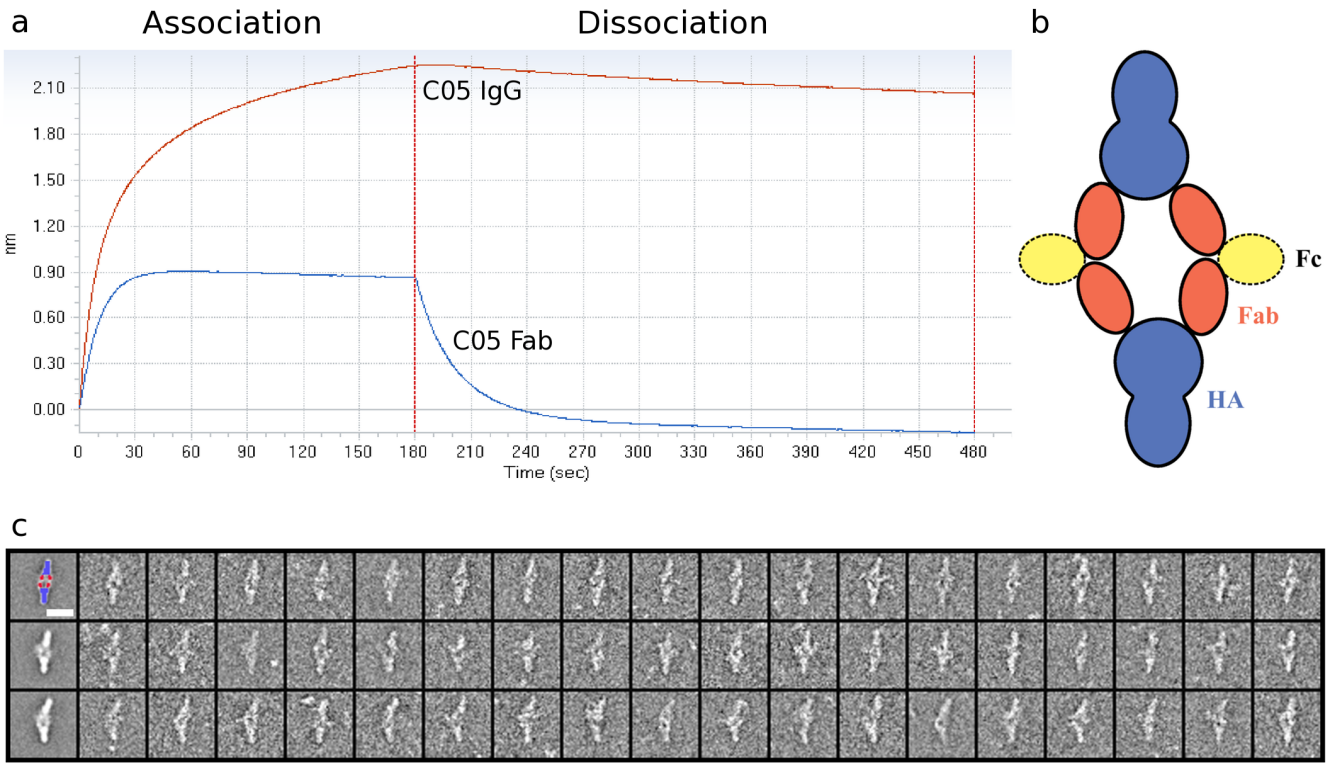

Supplementary Figure 3: C05 IgG binds HA with higher affinity than Fab and may cross-link adjacent HA trimers. **a,** BLI traces for the binding of C05 Fab (blue, 1uM combining sites) and IgG (red, 1uM combining sites) to immobilized A/Panama/2007/1999 (H3N2) HA. **b**, Schematic representation of two C05 IgGs cross-linking two H3 HA ectodomains, as seen in negative-stain EM 2D classes averages below. The HA is in blue, C05 Fab regions in red, and C05 Fc regions in yellow. The dotted border of the Fc region denotes regions that are disordered due to flexibility in the EM analysis in (**c**). **c**, Negative-stained reference-free 2D class averages of C05 IgG cross-linking two HAs compared to raw particles. First column entries represent reference free class averages. Remaining column entries are CTF corrected raw particles belonging to each class average. The first entry in the first column has been colored by component for HA (blue) and C05 Fab (red), as in (**b**). The scale bar is 100Å. In each class average, two IgGs can be seen cross-linking two HAs through interactions with the receptor-binding domain. The Fc region for each IgG, which is averaged out due to flexibility, is demarcated by the dashed outline in the cartoon diagram.

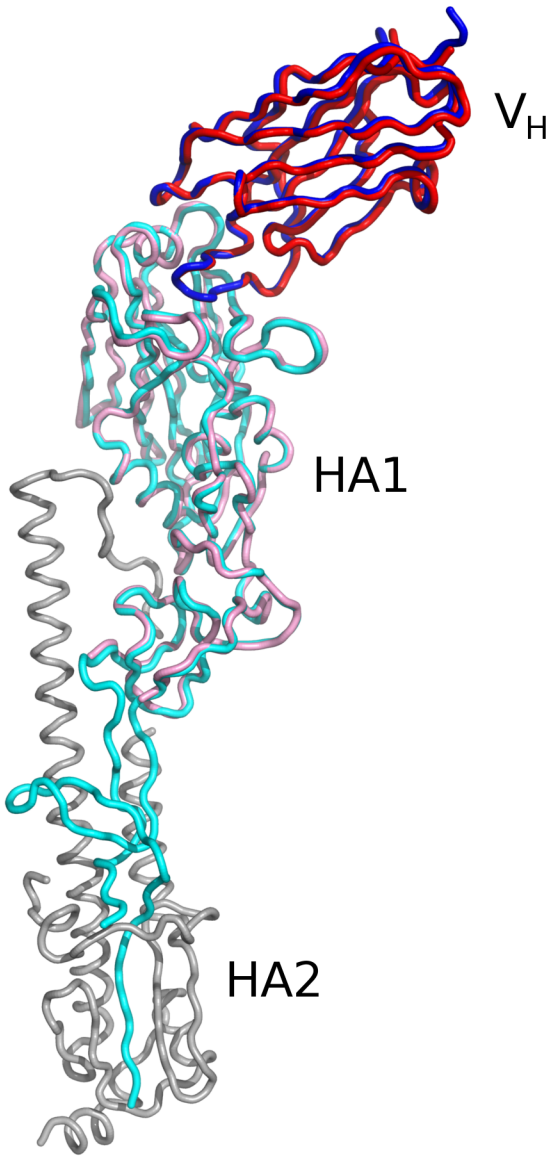

Supplementary Figure 4: C05-HA1 complex is very similar to the C05-trimer complex. Superposition of the C05-HA1 fragment complex (HA1 in pink, C05 V_H in red) onto the C05-HA trimer structure (HA1 in cyan, HA2 in gray, C05 V_H in blue). For clarity, only one protomer from the trimeric HA and only the V_H domains of C05 from both structures are shown.

a

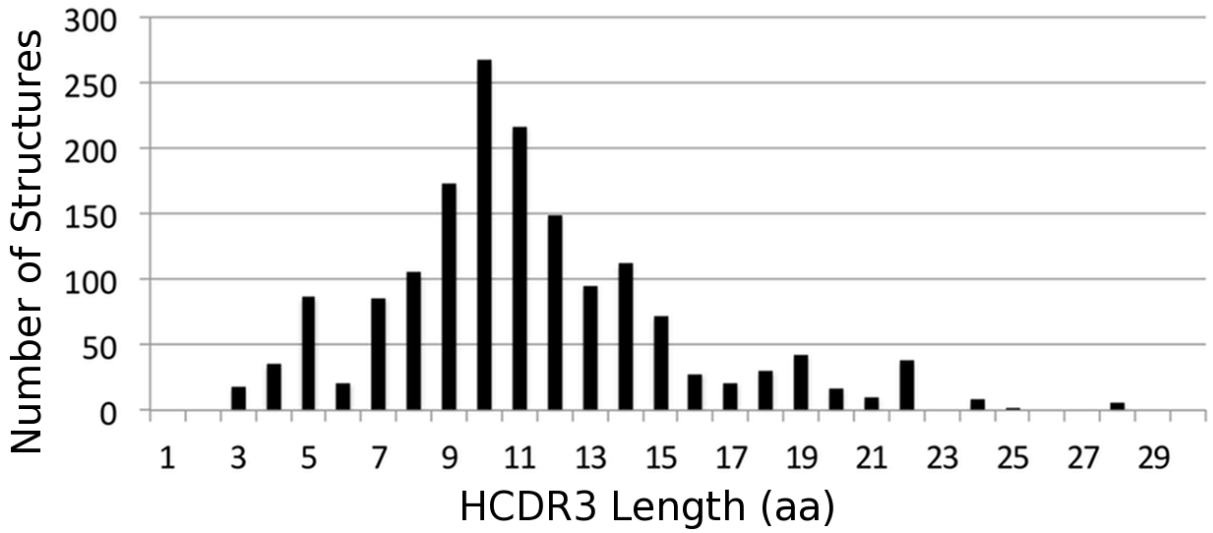

b

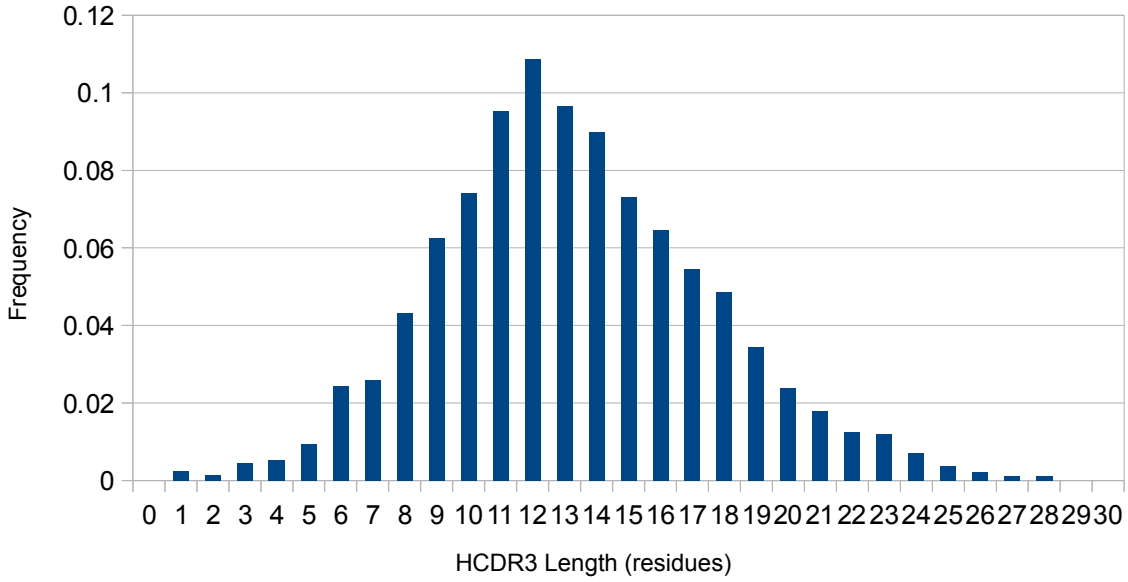

Supplementary Figure 5: Distribution of HCDR3 lengths in antibodies. **a,** Distribution of HCDR3 lengths in antibody structures deposited in the Protein Data Bank (PDB) as of Nov. 2011. At 24 residues in length, the HCDR3 of C05 is longer than nearly all other antibodies in the PDB. **b**, Distribution of HCDR3 lengths in all human antibodies in the Abysis database[1]. Approximately 1.5% of human antibodies have HCDR3 loops of 24 residues or longer.

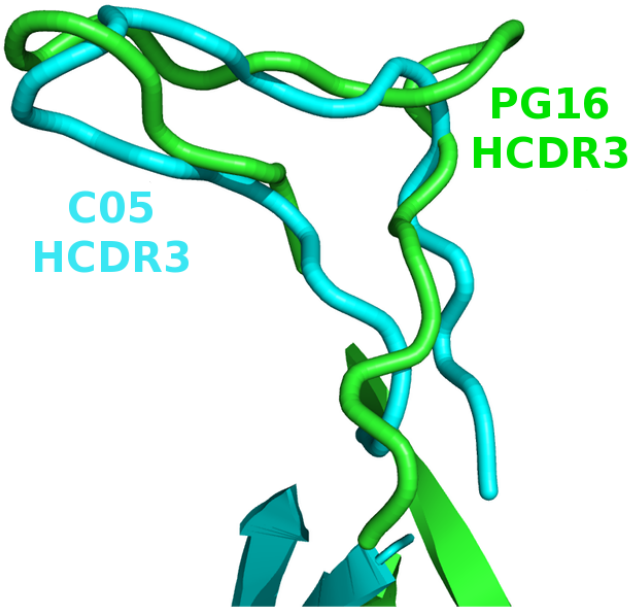

Supplementary Figure 6: C05 HCDR3 resembles the PG16 "hammerhead". To a first approximation, the long HCDR3 of C05 is similar to the "hammerhead" conformation observed in the anti-HIV mAb PG16. The longer HCDR3 from PG16 (28aa for PG16 compared to 24 a.a. for C05) has two well-defined branches and a more pronounced T-shape, while that of C05 has one long branch and a bulge and is more L-shaped.

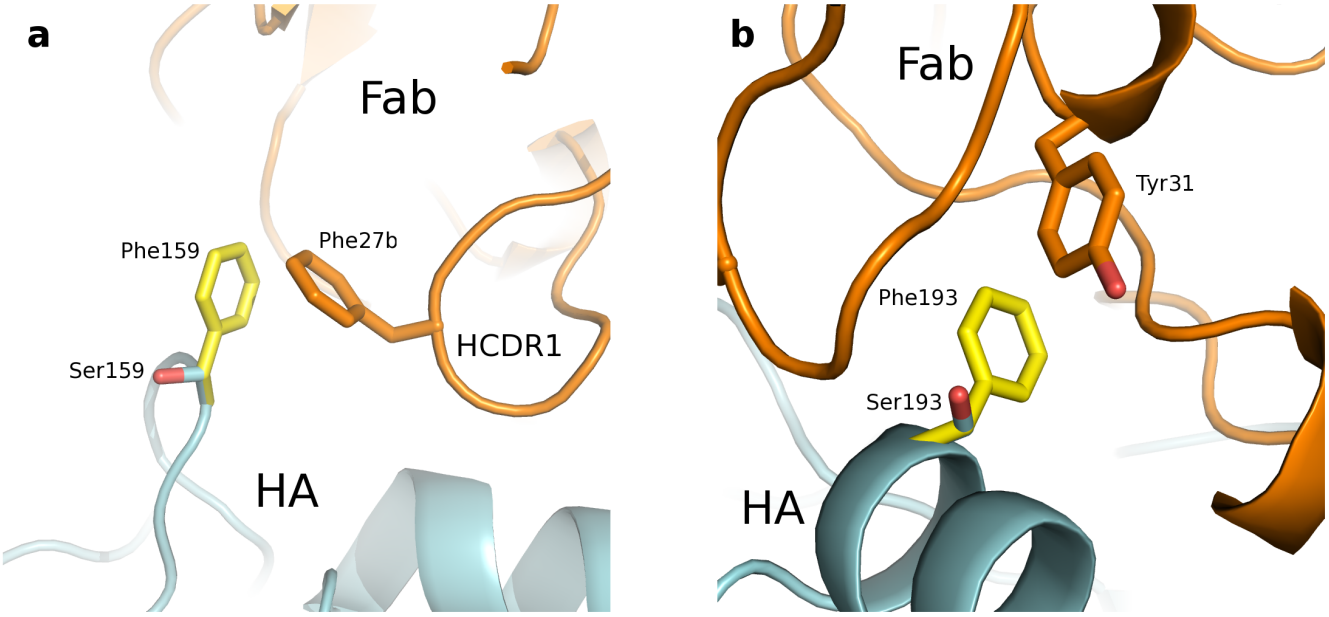

Supplementary Figure 7: Possible interaction between C05 HCDR1 and Phe159 in A/Perth/16/2009 (H3N2). a, In A/Hong Kong/1/1968, Ser159 (cyan sticks) is unable to make significant interactions with Phe27b (orange sticks) on C05, and mutation of Phe27b to Ala has no effect on binding. In contrast, the Phe27bAla mutation drastically reduces C05 binding to A/Perth/16/2009 (H3N2), where Phe159 on the HA (modeled on the C05-HK68 complex structure as yellow sticks) may make favorable stacking interactions with Phe27b. **b**, C05 Tyr31 is dispensable for binding to A/Hong Kong/1/1968 (H3N2), when it is opposite Ser193 on HA. Mutation of Tyr31 to Leu or Ala decreases C05 affinity for A/Perth/16/2009 (H3N2), where a Phe at position 193 may stack against Tyr31. However, Phe193Asn and Phe193Lys Perth09 mutants are bound with comparable affinity (see Fig. S11), suggesting that Tyr31 is not making a key, specific contact with HA, but may instead stabilize the HCDR1 loop. Phe193Asp, however, reduces C05 binding ~10-fold, perhaps due to electrostatic repulsion with the nearby Glu27d on HCDR1.

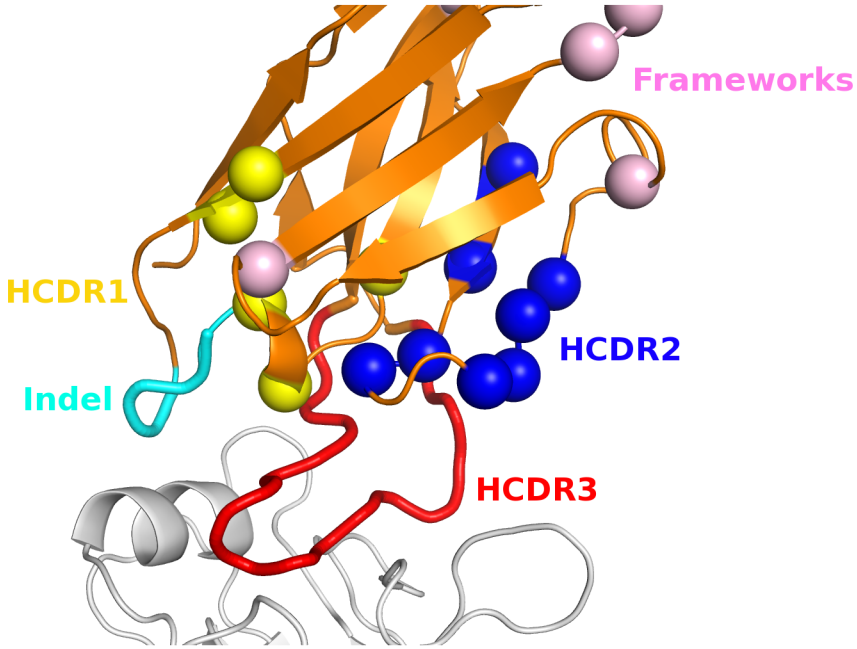

Supplementary Figure 8: Distribution of somatic hypermutations across the V_H domain of C05. Somatic mutations from the V_H3-23 germline were mapped onto the C05 complex structure and are indicated by spheres and color coded by their locations (HCDR1 in yellow, HCDR2 in blue, and framework regions in pink). The somatic insertion in HCDR1 is highlighted in cyan, and HCDR3 is colored red. The epitope region on HA is in white, at bottom. The density of somatic mutations is greatest near the tip of HCDR2, which lies just above HCDR3 and, along with somatic mutations in HCDR1, may help to support the conformation of HCDR3 and its interaction with HA. In addition, HCDR1 makes sequence-independent interactions between the backbone and HCDR3, possibly explaining why many substitutions in HCDR1 have only minimal effects on C05 binding. Approximately 500 and 250 $Å^2$ are buried between HCDR1-HCDR3 and HCDR2-HCDR3, respectively.

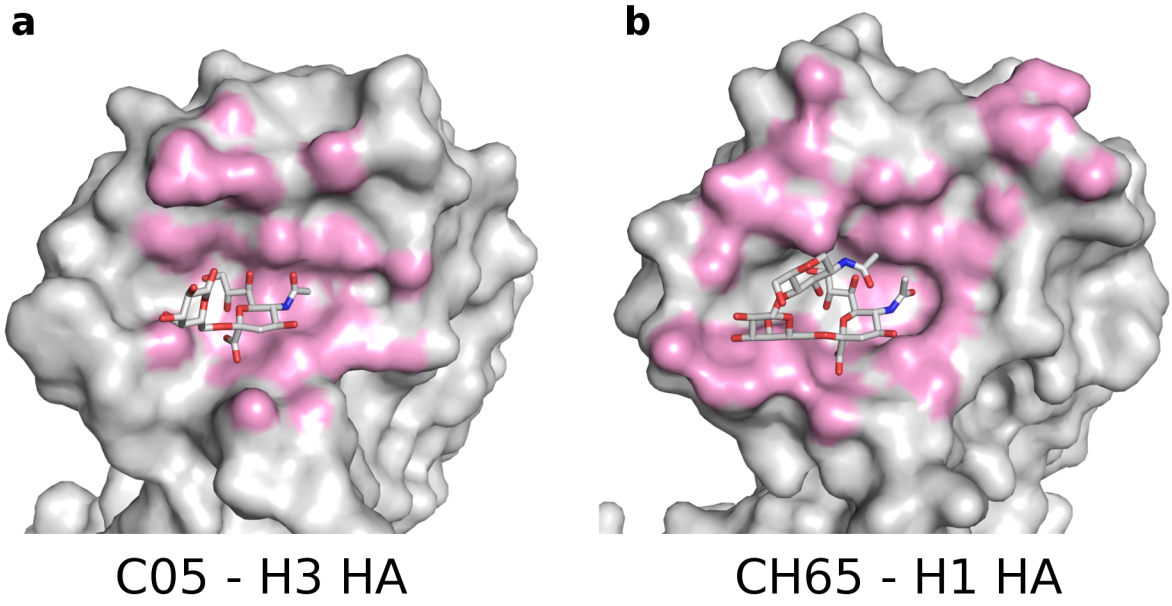

Supplementary Figure 9: Comparison of C05 and CH65 footprints on HA. HA atoms contacting C05 (**a**) or CH65 (**b**, derived from PDB code 3SM5 [2]) are mapped onto a surface representation of the HA1 subunit (pink coloring). The orientation of the HA is approximately identical in **a** and **b**. For reference, a human sialic acid receptor is depicted in the receptor binding site (white sticks, derived from PDB codes 1MQN [3] and 1RVZ [4] in **a** and **b**, respectively). Note the more extensive footprint of CH65 on HA, extending well outside the receptor-binding site (e.g., compare upper right region in **a** and **b**).

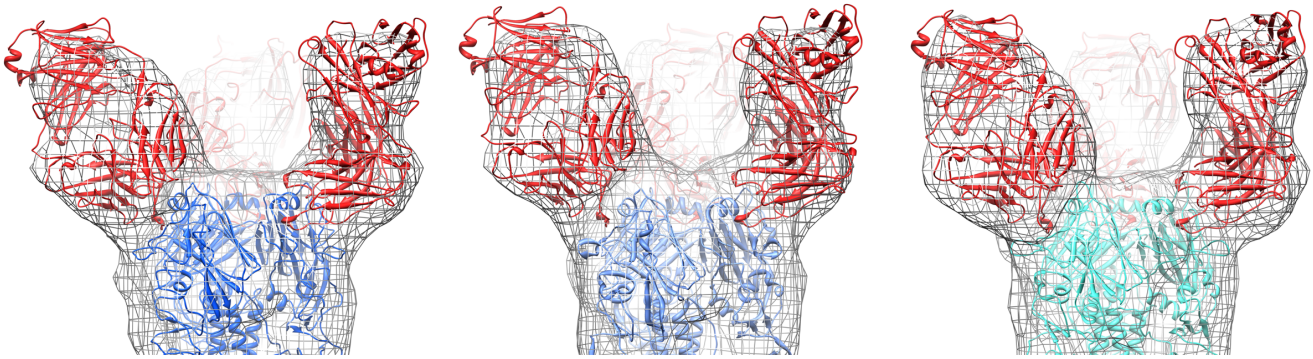

Supplementary Figure 10: Close up view of EM based models in Figure 3b highlighting the conserved interaction between C05 Fab and H1, H2, and H3 HAs (from left to right).

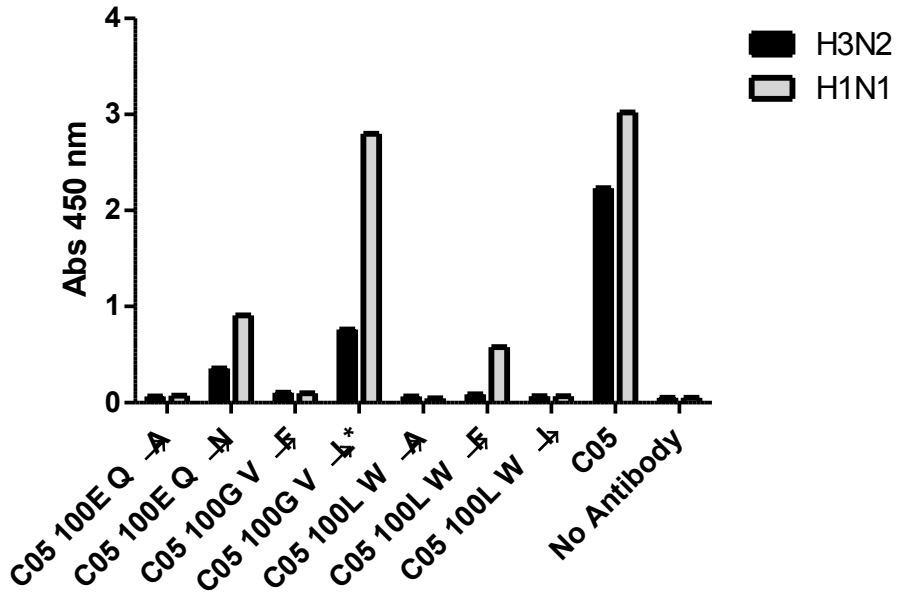

Supplementary Figure 11: Site directed mutations in C05 HCDR3 disrupt binding to both H1 and H3 subtype HA proteins. Amino-acid positions predicted to stabilize C05 HCDR3 structure or to be involved in binding were replaced with alanine or by a conservative substitution. Binding of WT and mutant C05 Fabs at 100 nM (except * which used 90 nM) was assessed by ELISA on plates coated with recombinant H1N1 New Caledonia/20/1999 or H3N2 Wisconsin/67/05 HA proteins (Protein Sciences) and detected with anti-kappa-HRP antibodies.

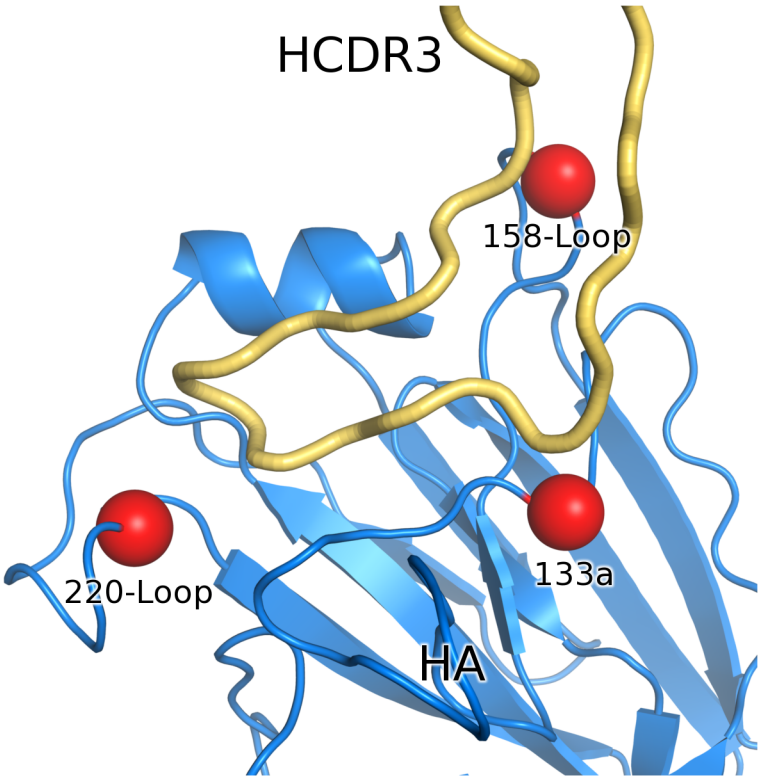

Supplementary Figure 12: Insertions and deletions near the C05 epitope. In addition to the insertion at HA1 residue 133a that appears to restrict C05 binding to H5 and some H1 isolates, two other indels were identified in this study that may impact C05 binding. A large number of isolates have single or double amino-acid insertions around HA1 position 158 (158a, 158b). C05 makes minor contacts with the tip of this loop in the HK68 complex, and interaction with Phe159 appears to be critical for high affinity binding to Perth09 (Fig. S6). The crystal structure of H14 HA (PDB code 3EYK [5]), which has a single amino-acid insertion at 158a in the loop, suggests that even a single residue insertion can lead to significant clashes with bound C05, although flexibility in the loop may allow it to adopt a more favorable conformation. However, C05 binding to all HAs tested with a single or double insertion at 158a/158b was undetectable, including H4, H6, H7, H10, H14, and H15, consistent with insertions having a negative effect on binding. Finally, some H7 viruses and most sequenced H16 subtypes have deletions in the 220-loop, which lines one side of the receptor binding site (8 and 1 amino-acid deletions, respectively). A crystal structure of an H7 HA with the 8 amino-acid deletion reveals that the region surrounding HA residue 226 is completely excised (PDB code 3M5G[6]). The single residue deletion in H16 likely has a more subtle effect, and it is unclear whether this impacts C05 binding. Together, indels at positions 133a, 158a/158b, and in the 220-loop may reduce or eliminate C05 activity against the H4, H5, H6, H7, H10, H14, H15, and H16 subtypes, and restrict the susceptible H1 isolates to ~34% of the total sequences and should be taken into consideration in design of immunogens.

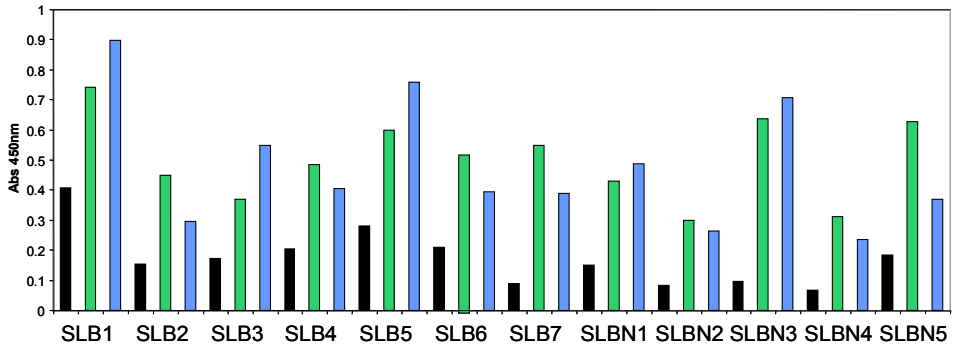

Supplementary Figure 13: Influenza survivors donating serum for library construction have high reactive titers to H1N1 A/New Caledonia/20/1999 and H3N2 A/Panama/2007/1999 hemagglutinin proteins. Serum ELISA analysis on purified recombinant hemagglutinin proteins at 1:10,000 demonstrates the presence of high titer anti-hemagglutinin antibodies in each of 12 survivors (SLB1-7 and SLBN1-5). Reactivity to H5N1 A/Vietnam/1203/2004, included as a control, is lower across all donors. Black bars- A/Vietnam/1203/04 hemagglutinin-coated wells, Green bars- A/New Caledonia/20/1999 coated wells, Blue bars- A/Panama/2007/1999 coated wells. No reactivity was observed to uncoated wells (data not shown).

Supplementary Figure 14: Biolayer interferometry binding curves and reported K_d values for C05 binding to various HAs. Presented in each plot are the observed association and dissociation curves at multiple concentrations of Fab (blue lines) and the best fit curves (red) resulting in the reported K_d values.

C05 vs A/Perth/16/2009 (H3N2) K_d = 15nM

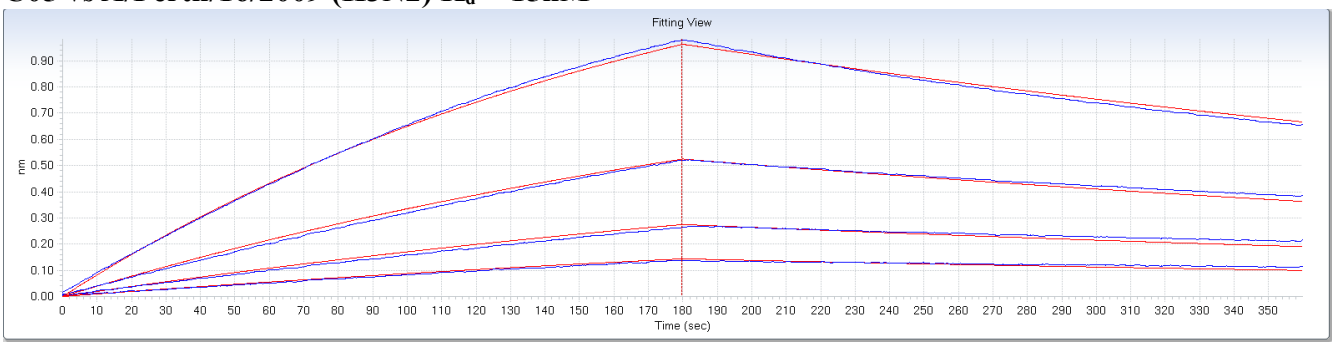

C05 vs A/Hong Kong/1/1968 (H3N2) K_d = 430nM

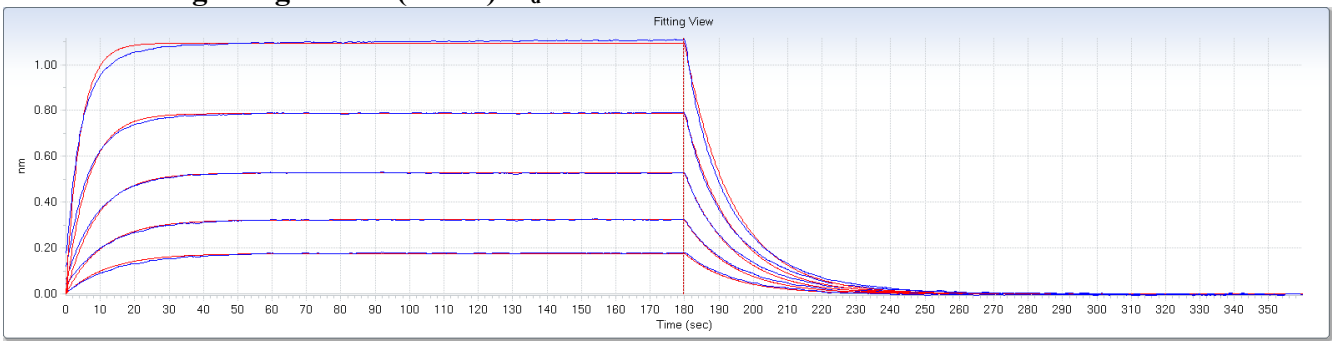

C05 vs A/Panama/2007/1999 (H3N2) K_d = 72nM

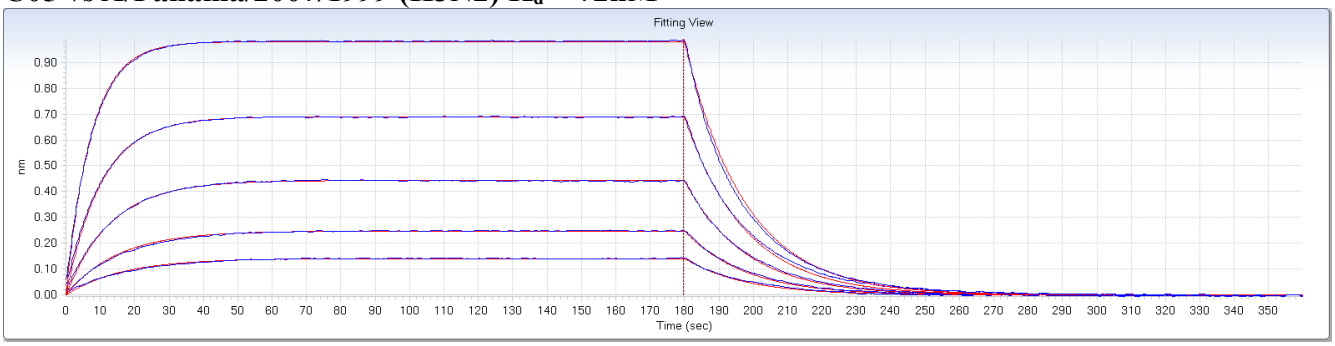

C05 vs A/Perth/16/N133S/2009 (H3N2) K_d = 15nM

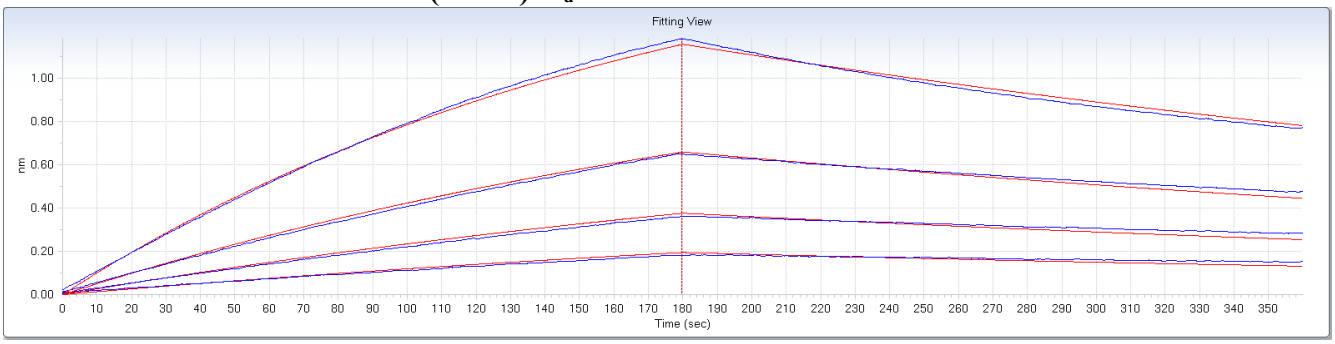

C05 vs A/Perth/16/T135K/2009 (H3N2) K_d = 3.9nM

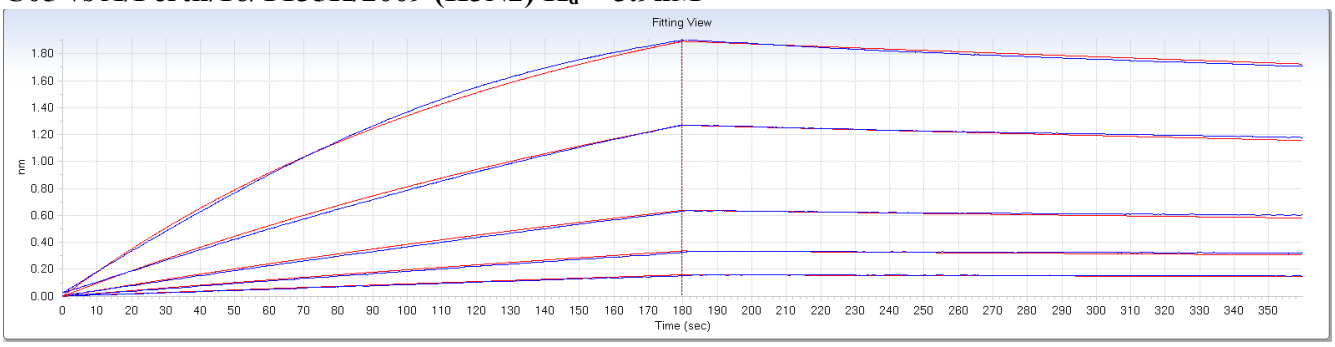

C05 vs A/Perth/16/F193D/2009 (H3N2) K_d = 110nM

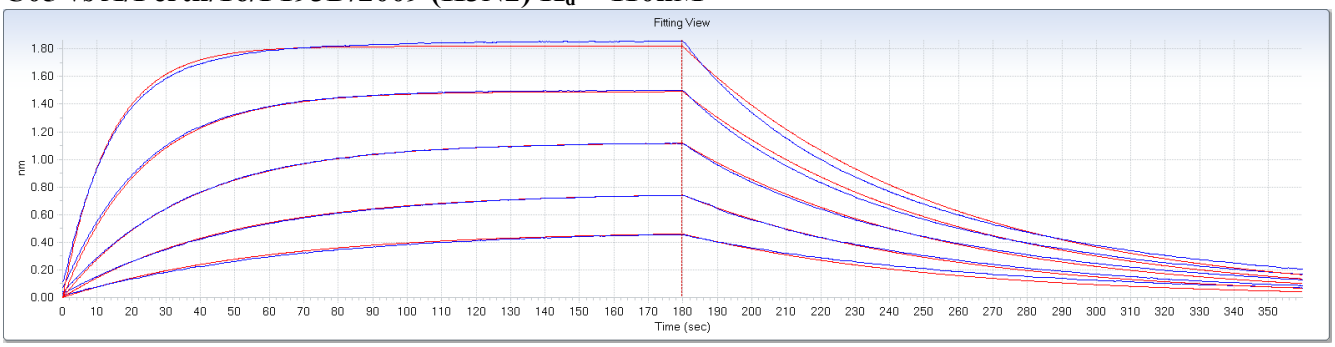

C05 vs A/Perth/16/F193N/2009 (H3N2) K_d = 5nM

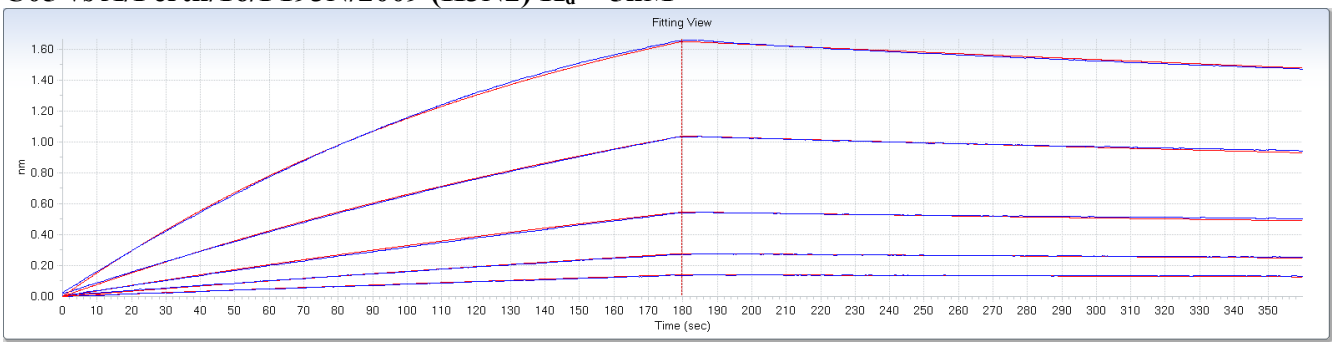

C05 vs A/Perth/16/F193K/2009 (H3N2) K_d = 44nM

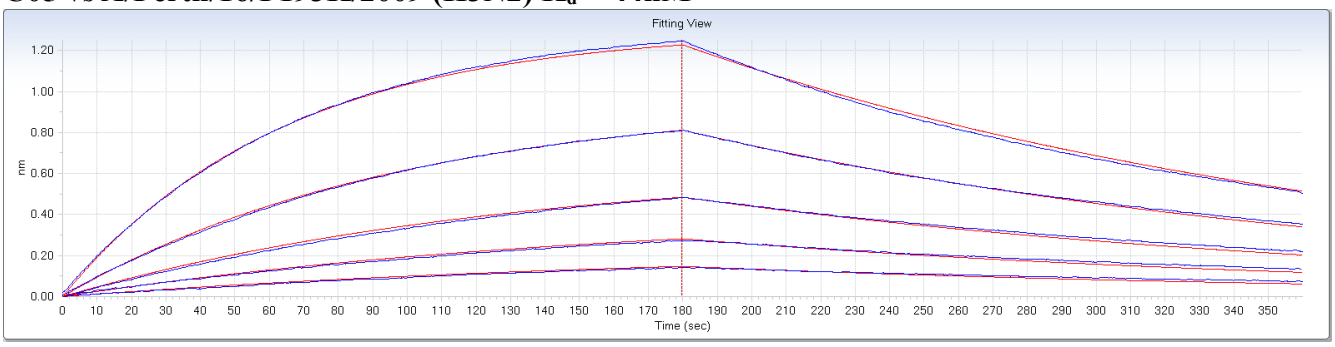

Supplementary Figure 15: Biolayer interferometry binding curves and reported K_d values for C05 mutant binding to HK68 and Perth09 H3 HAs. Presented in each plot are the observed association and dissociation curves at multiple concentrations of Fab (blue lines) and the best fit curves (red) resulting in the reported K_d values.

$C05^{wt}$ vs A/Perth/16/2009 (H3N2) K_d = 18nM

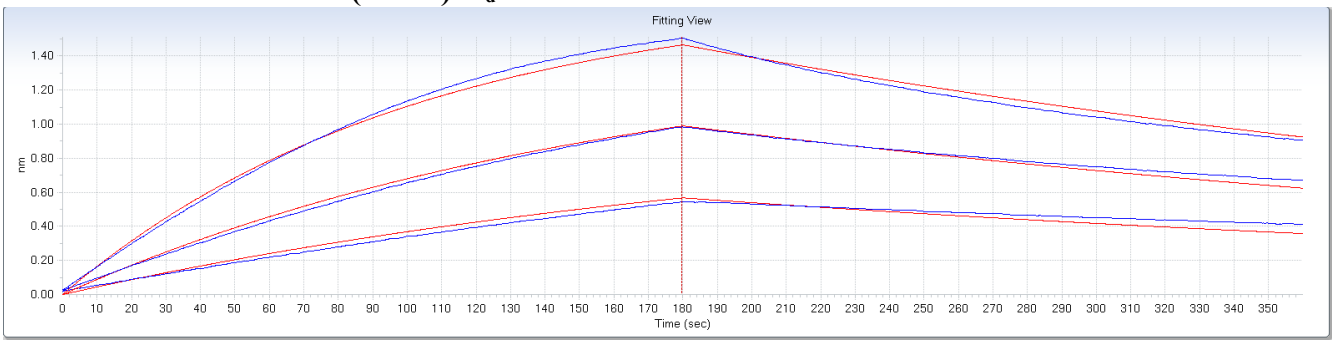

delC05 vs A/Perth/16/2009 (H3N2), 2:1 Binding, K_{d1} = 1300nM*, K_{d2} = 130nM*

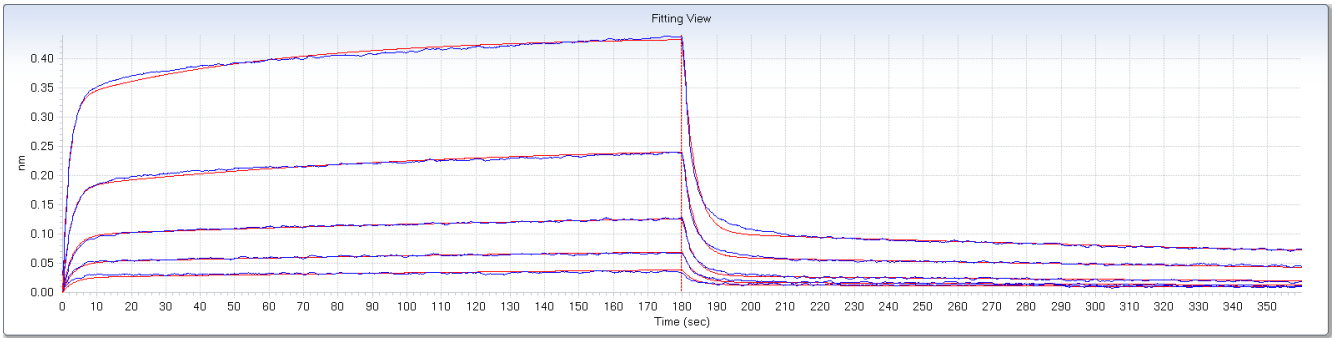

** Binding curves for the delC05 mutant could only be fit with a 2:1 model, with apparent K_{d1} = 1300nM, K_{d2} = 130nM. Overall, most of the binding is explained by the faster, lower affinity process (K_{d1} = 1300nM). The slower process may reflect non-specific interaction of the Fab with the sensor at the high concentrations required to obtain good binding in this experiment. While wild-type C05 and most of the other mutants show no signs of non-specific interaction with the sensor, the relatively drastic mutation in delC05 (5 residue deletion) may have increased the Fab's tendency stick to surfaces. Thus, we regard the K_{d1} = 1300nM as the most relevant binding constant for this interaction, which is on par with the affinity of key point mutations in C05 (e.g., Phe27bAla, Tyr31Ala) that also disrupt the interactions between HCDR1 and HA.

$C05^{Phe27bAla}$ vs A/Perth/16/2009 (H3N2) K_d = 460nM

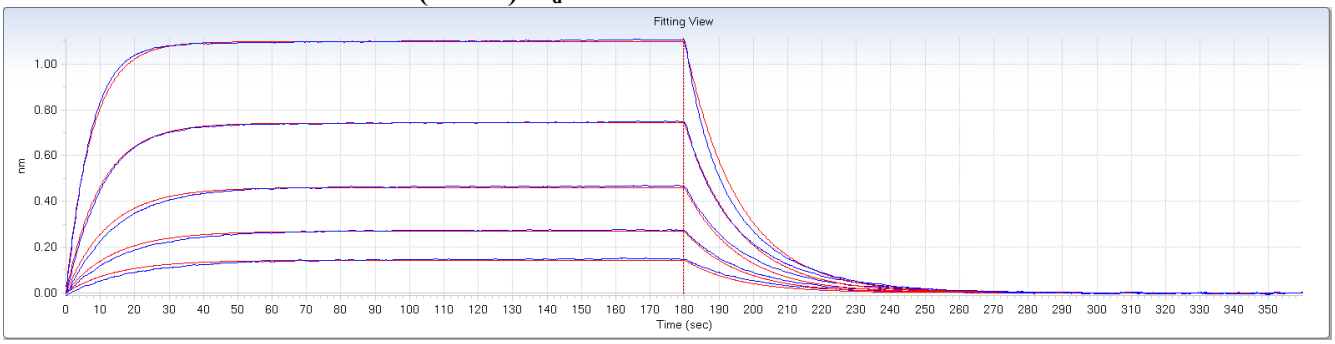

C05^{Gly27cAla} vs A/Perth/16/2009 (H3N2) K_d = 33nM

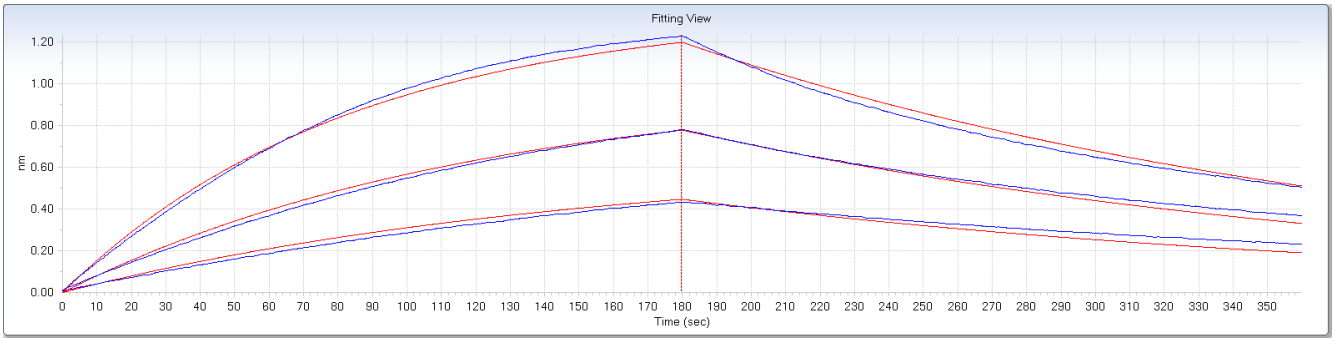

C05^{Glu27dAla} vs A/Perth/16/2009 (H3N2) K_d = 28nM

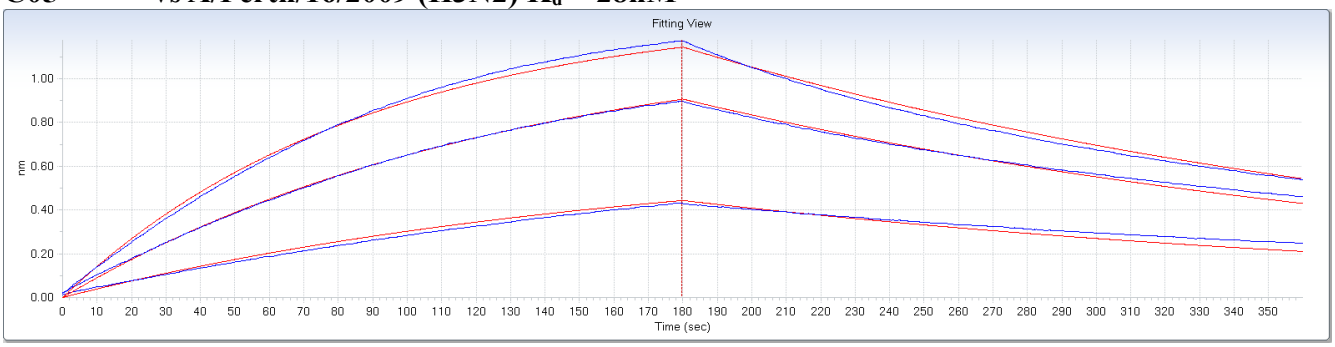

C05^{Tyr31Phe} vs A/Perth/16/2009 (H3N2) K_d = 6.8nM

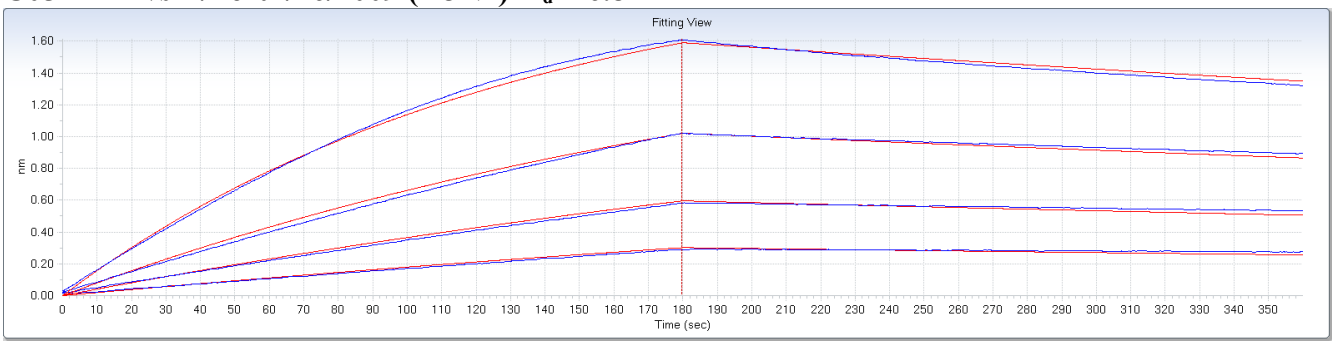

C05^{Tyr31Leu} vs A/Perth/16/2009 (H3N2) K_d = 560nM

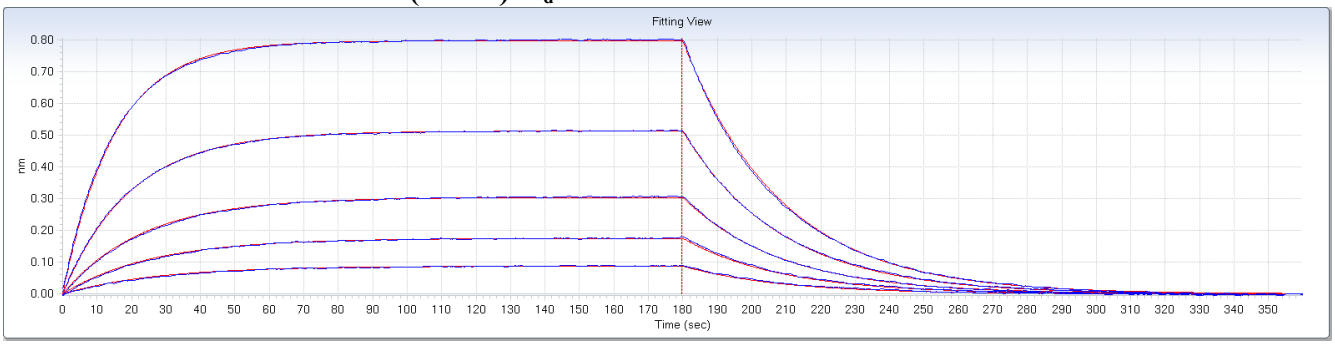

C05^{Tyr31Ala} vs A/Perth/16/2009 (H3N2) K_d = 550nM

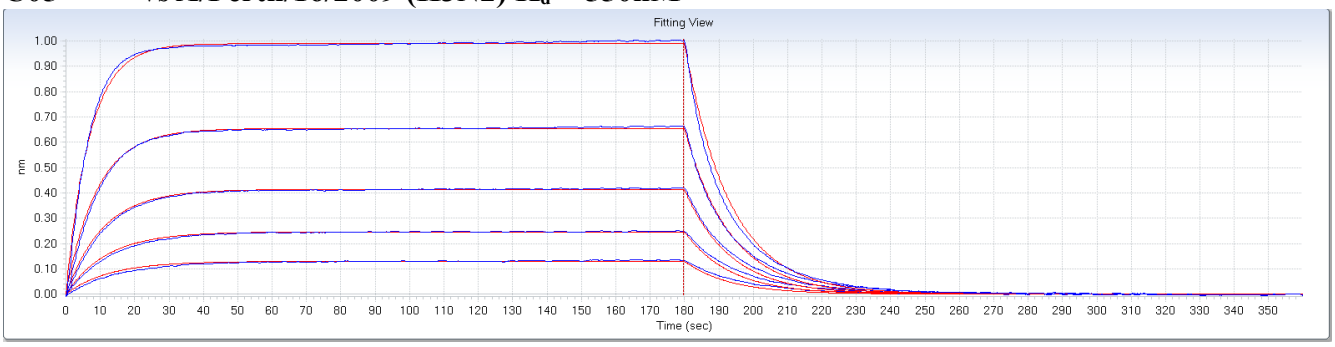

C05^{wt} vs A/Hong Kong/1/1968 (H3N2) K_d = 500nM

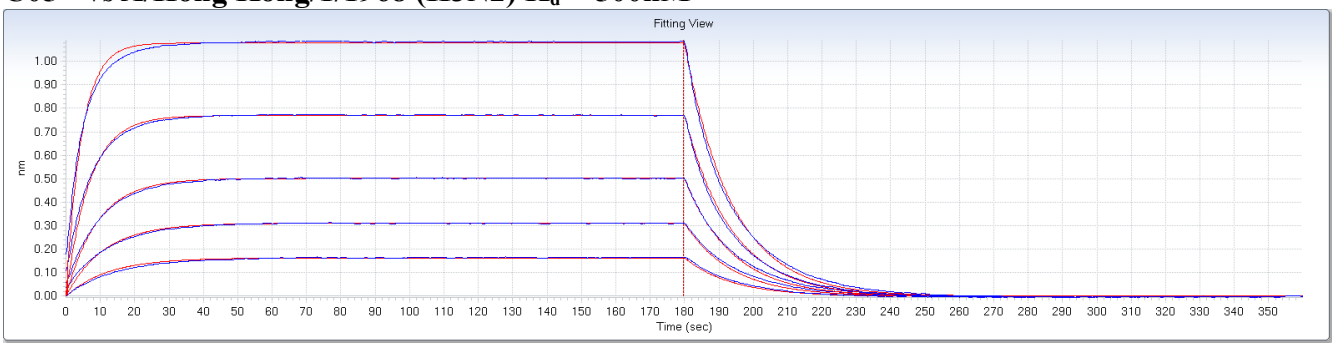

delC05 vs A/Hong Kong/1/1968 (H3N2) K_d = 690nM

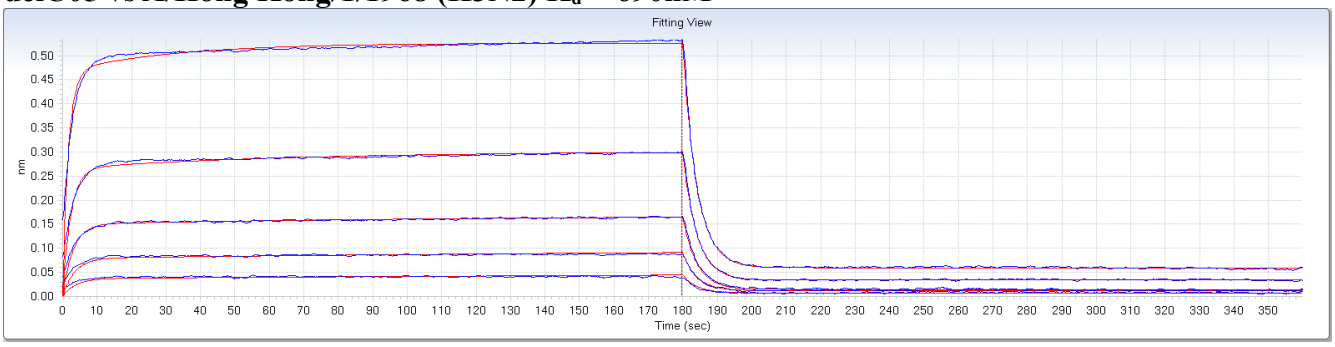

C05^{Phe27bAla} vs A/Hong Kong/1/1968 (H3N2) K_d = 610nM

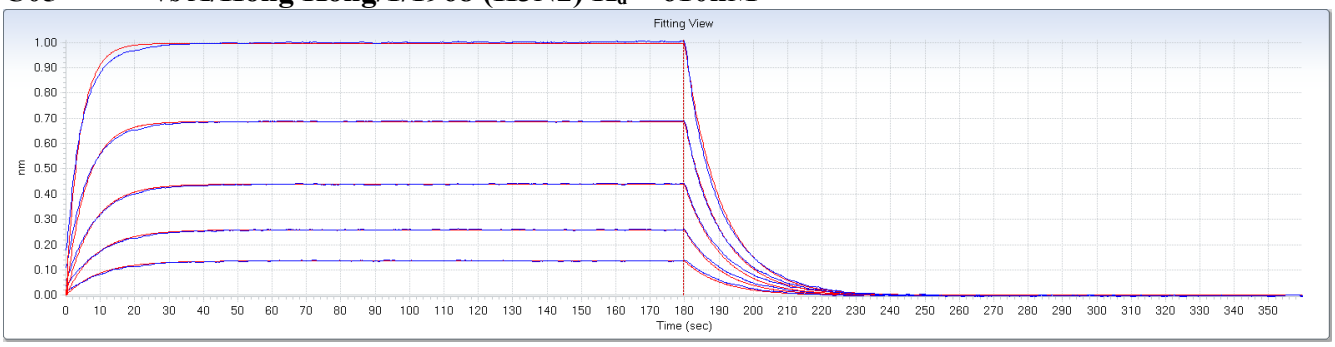

C05^{Gly27cAla} vs A/Hong Kong/1/1968 (H3N2) K_d = 450nM

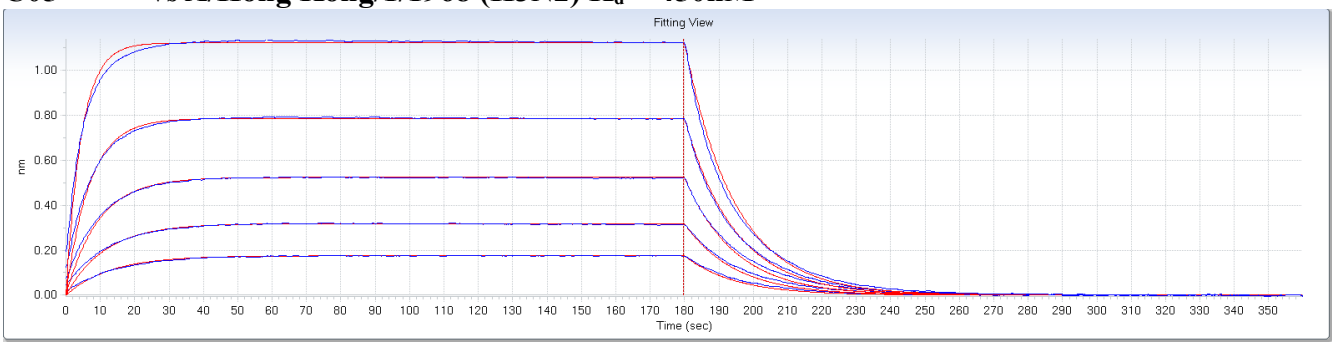

C05^{Glu27dAla} vs A/Hong Kong/1/1968 (H3N2) K_d = 540nM

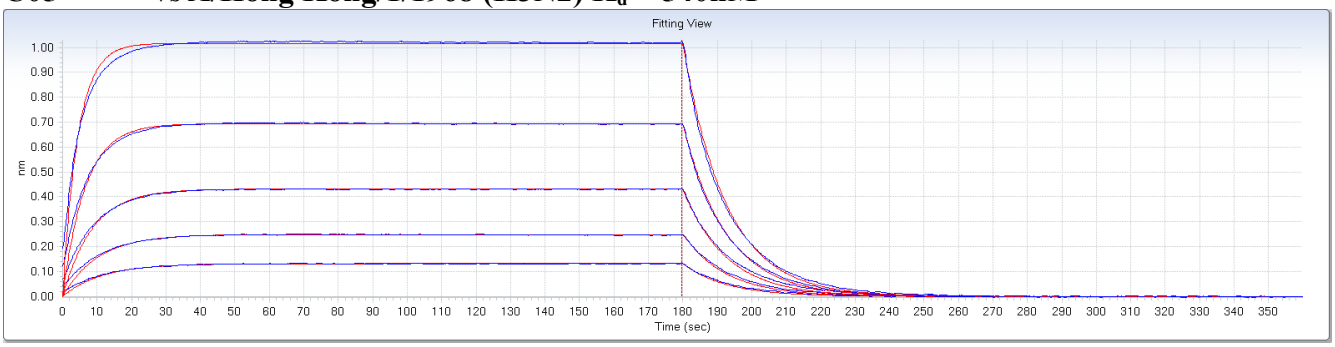

C05^{Tyr31Phe} vs A/Hong Kong/1/1968 (H3N2) K_d = 420nM

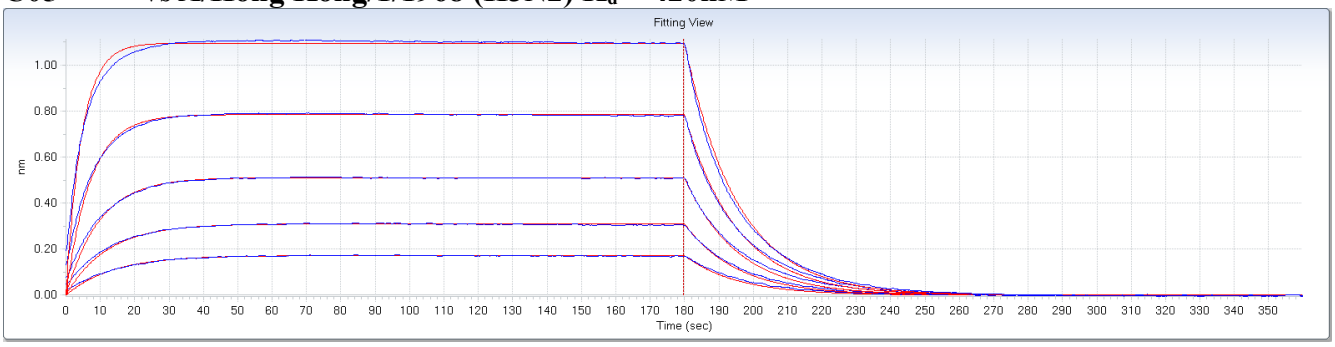

C05^{Tyr31Leu} vs A/Hong Kong/1/1968 (H3N2) K_d = 1400nM

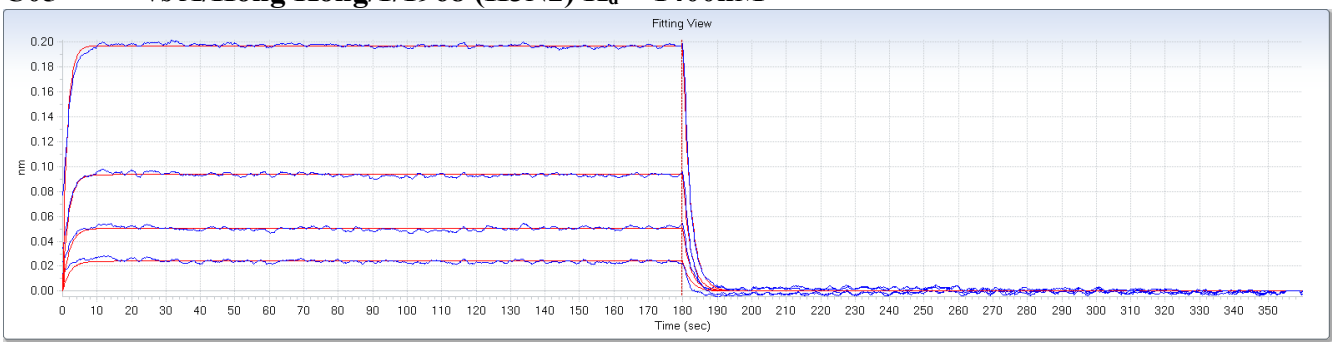

C05^{Tyr31Ala} vs A/Hong Kong/1/1968 (H3N2) K_d = 640nM

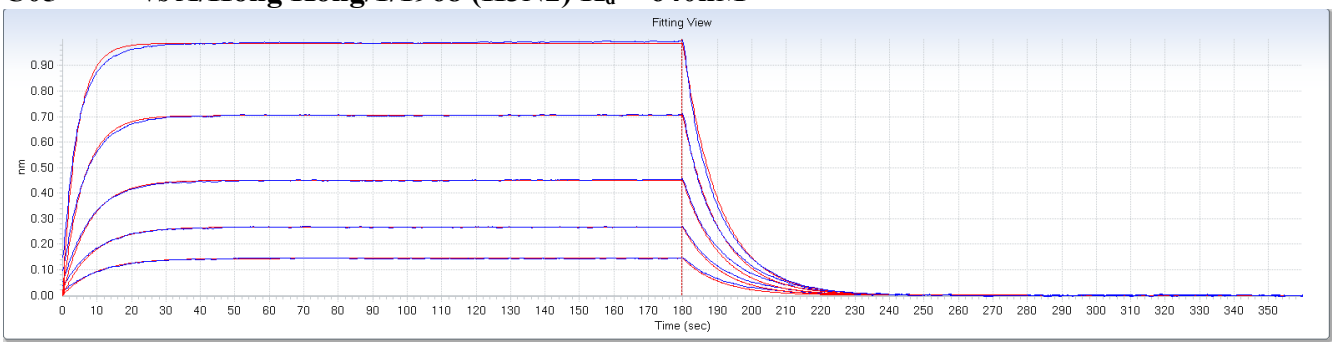

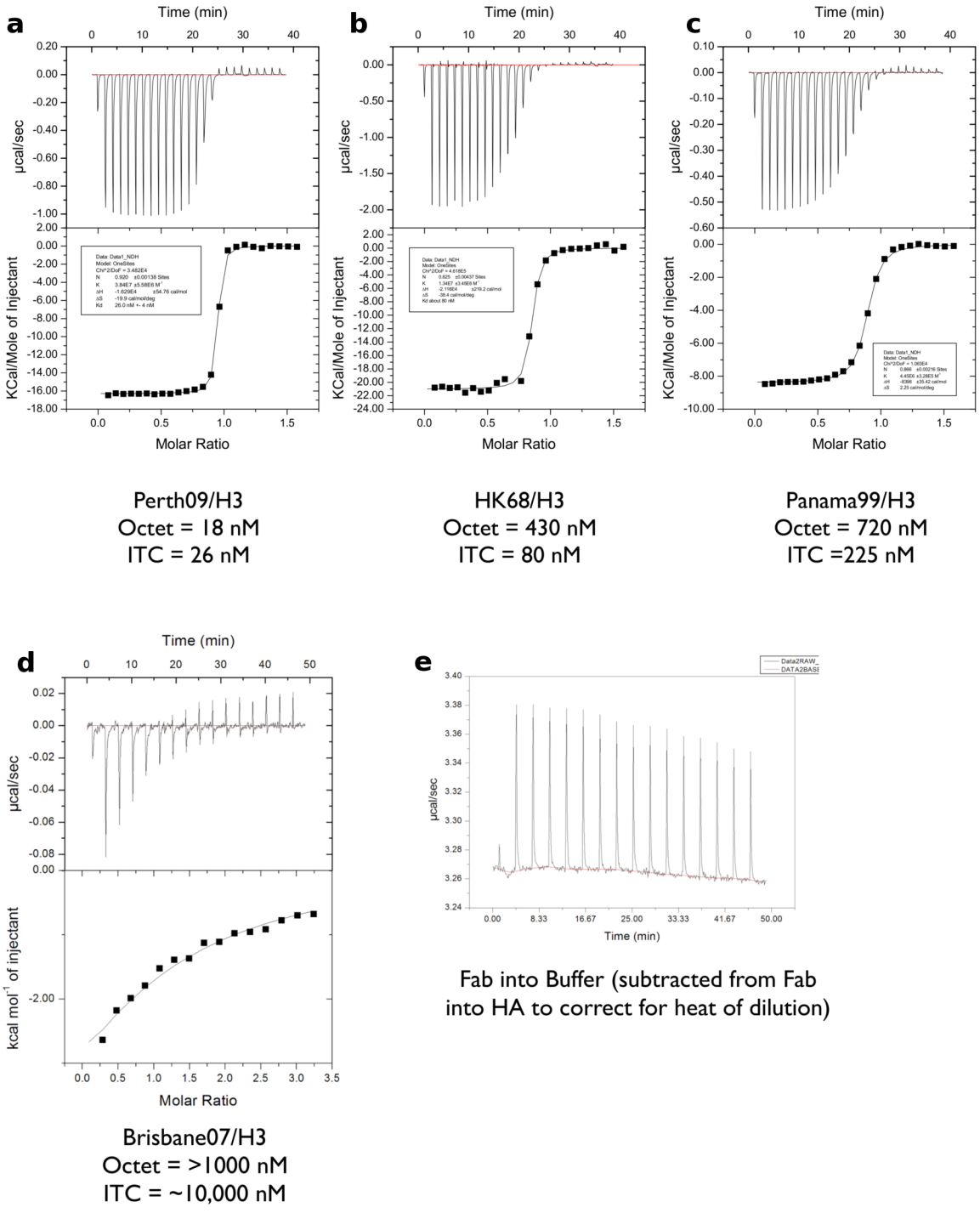

Supplementary Figure 16: Isothermal titration calorimetry isotherms for reported values of K_d. Data for C05 binding to (**a**) A/Perth/16/2009 (H3N2), (**b**) A/Hong Kong/1/1968 (H3N2), (**c**) A/Panama/2007/1999 (H3N2), and (**d**) A/Brisbane/10/2007 (H3N2). To correct for the heat of dilution of C05 Fab into the cell, Fab was titrated into buffer alone and subtracted from the Fab into HA experiments. A representative titration (used for the correction of the C05 - A/Brisbane/10/2007 (H3N2) titration) is shown in (**e**).

Supplementary Table 1: Data collection and refinement statistics.

Data collection	HK68/H3 HA	C05 Fab	C05-HK68 HA1	C05-HK68 Trimer
Beamline	SSRL 11-1	APS 23ID-D	APS 23ID-D	APS 23ID-B
Wavelength (Å)	1.067	1.033	1.033	1.033
Space group	$C222_1$	$P4_12_12$	$P2_1$	P1
Unit cell parameters (Å, °)	a=105.1, b=151.5, c=347.8, α=β=γ=90	a=b=160.1, c=135.5, α=β=γ=90	a=90.4, b=246.5, c=94.4, α=γ=90, β=91.4	a=142.6, b=160.8, c=181.4, α=88.7, β=83.1, γ=82.6
Resolution (Å)	50-1.90 (1.97-1.90)[a]	50-2.30 (2.40-2.30)[a]	50-2.95 (3.06-2.95)[a]	50-4.10 (4.20-4.10)[a]
Observations	1,350,595	1,071,794	262,281	199,215
Unique Reflections	215,875	78,741	84,287	88, 441
Redundancy	6.3 (3.6)[a]	13.2 (7.7)[a]	3.1 (3.0)[a]	1.5 (0.9)[a]
Completeness (%)	99.6 (97.3)[a]	99.9 (99.6)[a]	95.5 (97.2)[a]	78.7 (53.4)[a]
$\langle I/\sigma_I \rangle$	14.1 (1.8)[a]	20.4 (2.2)[a]	10.9 (2.1)[a]	5.3 (1.9)[a]
R_{sym}[b]	0.15 (0.65)[a]	0.19 (0.80)[a]	0.10 (0.58)[a]	0.16 (0.34)[a]
R_{pim}[b]	0.07 (0.28)[a]	0.05 (0.30)[a]	0.06 (0.25)[a]	0.15 (0.32)[a]
Z_a[c]	3	2	4	12
Refinement statistics				
Resolution (Å)	50-1.90	50-2.30	50-2.95	50-4.10
Reflections (work)	204,574	74,300	80,018	85,047
Refections (test)	10,817	3,937	4,191	4,524
R_{cryst}(%)[d] / R_{free}(%)[e]	16.2 / 18.9	21.2 / 24.0	21.2 / 24.1	30.9 / 33.4
Average B (Å^2)	26.6	44.7	83.8	55.7
Wilson B (Å^2)	21.0	52.0	69.9	74.2
Protein atoms	12,000	6,833	22,342	89,436
Carbohydrate atoms	416	0	56	1356
Waters	1707	519	0	0
Other	42	8	8	0
RMSD from ideal geometry				
Bond length (Å)	0.014	0.003	0.005	0.008
Bond angles (°)	1.42	1.00	1.10	1.34
Ramachandran statistics (%)[f]				
Favored	96.4	97.8	97.3	98.0
Outliers	0.1	0.2	0.1	0.1
PDB Code	4FNK	4FNL	4FP8	4FQR

[a] Numbers in parentheses refer to the highest resolution shell.

[b] $R_{\mathrm{sym}} = \Sigma_{hkl} \Sigma_i \mid I_{hkl,i} - \langle I_{hkl} \rangle \mid / \Sigma_{hkl} \Sigma_i I_{hkl,I}$ and $R_{\mathrm{pim}} = \Sigma_{hkl} (1/(n\text{-}1))^{1/2} \Sigma_i \mid I_{hkl,i} - \langle I_{hkl} \rangle \mid / \Sigma_{hkl} \Sigma_i I_{hkl,I}$, where $I_{hkl,i}$ is the scaled intensity of the i^{th} measurement of relection h, k, l, $\langle I_{hkl} \rangle$ is the average intensity for that reflection, and n is the redundancy[7]. Note that despite the high R_{sym} in the highest resolution shell, the high redundancy enables the average F's to be well determined (assuming measurement errors are randomly distributed), as reflected by the redundancy-independent measure of the quality of intensity measurements R_{pim}.

[c] Z_a is the number of HA monomers, Fabs or HA monomer-Fab complexes per crystallographic asymmetric unit.

[d] $R_{\mathrm{cryst}} = \Sigma_{hkl} \mid F_o - F_c \mid / \Sigma_{hkl} \mid F_o \mid \times 100$

[e] R_{free} was calculated as for R_{cryst}, but on a test set comprising 5% of the data excluded from refinement.

[f] Calculated using Molprobity[8].

Supplementary Table 2: Deletion of HCDR1 has little effect on binding to most HAs. Comparison of wildtype and del(FGEST) mutant C05 Fab binding to H1, H2, and H3 HAs by biolayer interferometry. +++, K_d ~ 10-100 nM; ++, K_d ~ 100-1000 nM; +, K_d ~ 1-10 uM. Only C05 binding to Perth09 is affected by the del(FGEST) deletion in HCDR1.

Subtype	Isolate	Relative Affinity	
		WT C05	delC05
H1N1	A/Beijing/262/1995	++	++
H1N1	A/Solomon Islands/3/2006	+++	+++
H2N2	A/Japan/305/1957	+	+
H3N2	A/Hong Kong/1/1968	+	+
H3N2	A/Perth/16/2009	+++	+

Supplementary Table 3: Buried surface area (BSA) on HA for neutralizing antibodies against the HA1 receptor binding domain.

Antibody	BSA on HA
HC63	520 Å^2
C05	550 Å^2
BH151	630 Å^2
CH65	650 Å^2
HC63	680 Å^2
HC45	730 Å^2
2D1	740 Å^2

Supplementary Table 4: Conservation of C05 epitope across human H1/H2/H3 influenza A viruses versus all 16 subtypes. Listed is the percent conservation of C05 contact residues on HA (relative to the most common residue in the dataset) among human H1, H2, and H3 viruses or among all 16 subtypes. At the bottom is the mean conservation of all C05 contacts on HA.

Residue	Human H1-H2-H3	All 16 Subtypes
98	100.0	99.9
131	45.1	28.2
133	76.1	49.5
134	100.0	99.9
135	62.2	57.3
136	100.0	99.8
137	61.7	44.4
145	55.1	45.4
153	100.0	99.9
155	45.0	36.5
156	48.2	56.5
189	41.7	37.1
190	99.0	93.8
192	41.8	46.5
193	71.4	38.7
194	99.8	99.9
226	62.4	76.3
Mean Conservation	71.1	65.3

References

1. Abysis Database. at <http://www.bioinf.org.uk/abysis/>
2. Whittle, J. R. R. *et al.* Broadly neutralizing human antibody that recognizes the receptor-binding pocket of influenza virus hemagglutinin. *Proc. Natl. Acad. Sci. U.S.A.* **108**, 14216–14221 (2011).
3. Ha, Y., Stevens, D. J., Skehel, J. J. & Wiley, D. C. X-ray structure of the hemagglutinin of a potential H3 avian progenitor of the 1968 Hong Kong pandemic influenza virus. *Virology* **309**, 209–218 (2003).
4. Gamblin, S. J. *et al.* The structure and receptor binding properties of the 1918 influenza hemagglutinin. *Science* **303**, 1838–42 (2004).
5. Russell, R. J. *et al.* Structure of influenza hemagglutinin in complex with an inhibitor of membrane fusion. *Proc. Natl. Acad. Sci. U.S.A.* **105**, 17736–17741 (2008).
6. Yang, H., Chen, L.-M., Carney, P. J., Donis, R. O. & Stevens, J. Structures of receptor complexes of a North American H7N2 influenza hemagglutinin with a loop deletion in the receptor binding site. *PLoS Pathog.* **6**, e1001081 (2010).
7. Weiss, M. S. & Hilgenfeld, R. On the use of the merging R factor as a quality indicator for X-ray data. *J. Appl. Crystallog.* **30**, 203–205 (1997).
8. Chen, V. B. *et al.* MolProbity: all-atom structure validation for macromolecular crystallography. *Acta Crystallogr. D Biol. Crystallogr.* **66**, 12–21 (2010).